Unconventional transport properties of the itinerant ferromagnet $EuTi_{1-x}Nb_xO_3$ ($x = 0.10$–0.20)

Susmita Roy, Nazir Khan, and Prabhat Mandal
Saha Institute of Nuclear Physics, HBNI, 1/AF Bidhannagar, Calcutta 700 064, India

(Received 15 January 2018; revised manuscript received 6 September 2018; published 16 October 2018)

The detailed analysis of resistivity (ρ) for single-crystalline $EuTi_{1-x}Nb_xO_3$ ($x = 0.10$–0.20), an itinerant ferromagnet with very low Curie temperature (T_C), reveals that the charge conduction in this system is extremely sensitive to Nb concentration and dominated by several scattering mechanisms. Well below T_C, where the spontaneous magnetization follows Bloch's $T^{3/2}$ law, ρ exhibits T^2 dependence with a large coefficient ($\sim 10^{-1}$ $\mu\Omega$ cm K^{-2}) due to the electron-magnon scattering. Remarkably, all the studied samples exhibit a unique resistivity minimum at $T = T_{min}$, below which ρ shows a logarithmic increment with T (for $T_C < T < T_{min}$) due to the Kondo scattering of $4d^1$ itinerant electrons of Nb by the localized $4f$ moments of Eu^{2+} which suppresses strongly with applied magnetic field. In the paramagnetic state, T^2 and $T^{3/2}$ dependence of the resistivity have been observed, suggesting an unusual crossover from a Fermi-liquid to a non-Fermi-liquid behavior with increasing T.

DOI: 10.1103/PhysRevB.98.134428

I. INTRODUCTION

The interplay between magnetism and charge conduction in strongly correlated systems leads to several fascinating physical phenomena such as non-Fermi-liquid behavior, the Kondo effect, quantum phase transitions, the anomalous Hall effect, and large negative magnetoresistance (MR) [1–6]. Hence, any report of a new correlated itinerant ferromagnet immediately calls for exploring its magnetic and transport properties. Based on transport properties, metallic ferromagnets can be divided into two broad categories: (i) good metallic ferromagnets such as iron, nickel, and cobalt, which can be described by the Landau Fermi-liquid theory [7], and (ii) "bad metallic" ferromagnets such as heavy-fermion compounds and rare-earth transition-metal oxides [1,8–15]. For these so-called bad metals often the Fermi-liquid description breaks down due to strong electronic correlation. The celebrated itinerant-electron ferromagnets $SrRuO_3$ and $ZrZn_2$ can neither be classified as good metallic ferromagnets nor can they be compared with $3d$ transition-metal oxides like manganites [1,16,17].

There are a considerable number of theoretical and experimental works for understanding the nature of the orbital ground state in the perovskite titanate family $RTiO_3$ (where R = rare-earth ion) with a $3d^1$ electron configuration [18–21]. Among these titanates, $EuTiO_3$ is unique because, unlike other R ions, Eu is divalent ($4f^7$) and hence Ti is tetravalent ($3d^0$) [22–27]. Also, $EuTiO_3$ is an antiferromagnetic (AFM) ($T_N = 5.5$ K) [22–24] band insulator and quantum paraelectric with simple cubic structure while other titanates are Mott insulators [18–21]. The introduction of an electron into the Ti $3d$ orbital via the substitution of an R^{3+} ion at the Eu^{2+} site transforms $EuTiO_3$ into a ferromagnetic (FM) metal [22,24]. Except at low temperature, the T dependence of resistivity (ρ) for $Eu_{1-x}La_xTiO_3$ (ELTO) with $x = 0.10$ appears to be similar to 10% La-doped $SrTiO_3$ [22,24]. For $Sr_{0.9}La_{0.1}TiO_3$ (SLTO), ρ decreases smoothly down to very low temperature without showing any anomaly while a sharp drop in ρ is observed just below the FM transition (T_C) in ELTO. Most importantly, ELTO exhibits a weak upturn in ρ below ~30 K [22,24]. Another very promising candidate is obtained by substituting a Nb^{4+} ($4d^1$) ion at the Ti^{4+} ($3d^0$) site in $EuTiO_3$ without breaking the magnetic chains of Eu^{2+} moments. A notable increase in electrical conductivity is observed in $EuTi_{1-x}Nb_xO_3$ (ETNO) with the increase in Nb concentration (x) [25–28]. In contrast to ELTO, the substitution is done at the B site for ETNO and it shows metallic and FM behavior over a much wider range of Nb doping ($0.05 < x \leqslant 1$) [27,28]. Insulator-to-metal transition in ABO_3-type perovskite materials through B-site substitution is rare. Normally, B-site substitution creates disordering, which enhances carrier localization. In spite of some minor differences, the nature of the magnetism and transport properties in ELTO and ETNO are similar. Remarkably, ETNO also exhibits an upturn in ρ below 30 K [27]. Though ρ decreases with decrease in T for both ELTO and ETNO, it is quite unexpected that the mechanism of charge conduction in these two systems will be the same as that in SLTO. Due to the presence of large localized moments, there may be strong interaction between the $4d^1$ itinerant charge carrier and the spin ($S = 7/2$) of Eu^{2+}.

In order to shed some light on the charge conduction mechanism in $EuTi_{1-x}Nb_xO_3$, we report a comprehensive study of transport properties on high-quality single-crystalline samples with $x = 0.10$, 0.15, and 0.20. To the best of our knowledge, the detailed analysis of temperature and magnetic field dependence of resistivity for $EuTi_{1-x}Nb_xO_3$ or $Eu_{1-x}La_xTiO_3$ has not been done so far. The observed results are compared and contrasted with the different classes of FM metals mentioned above. Indeed, our detailed analysis of resistivity unveils the presence of several unusual scattering mechanisms. With increasing T, the charge scattering mechanism crosses over from electron-magnon to spin-disordering to Kondo to electron-electron scattering to an unusual $T^{3/2}$ dependence of resistivity due to non-Fermi-liquid behavior.

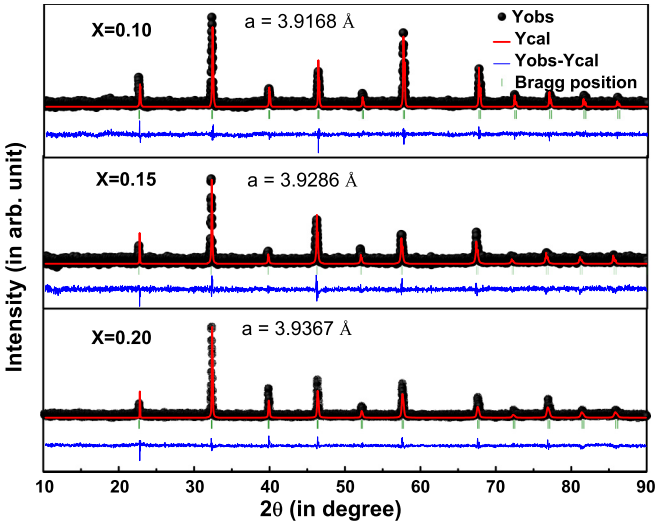

FIG. 1. X-ray powder diffraction patterns for $EuTi_{1-x}Nb_xO_3$ ($x = 0.10$–0.20) at room temperature. The solid red lines indicate the Rietveld refinements of the diffraction patterns.

II. SAMPLE PREPARATION AND EXPERIMENTAL DETAILS

Polycrystalline $EuTi_{1-x}Nb_xO_3$ ($x = 0.10$–0.20) powder samples were prepared by the standard solid-state reaction method. Stoichiometric mixtures of Eu_2O_3 (preheated), Nb_2O_5, and TiO_2 were heated at 1000–1100 °C for a few days in a reduced atmosphere containing 5% H_2 and 95% argon followed by intermediate grindings. The obtained powder was pressed into two cylindrical rods which were then sintered at 1100 °C in the same environment. The single crystals of $EuTi_{1-x}Nb_xO_3$ ($x = 0.10$, 0.15, and 0.20) were grown via the floating-zone technique in reduced atmosphere (5% H_2 and 95%) using a four-mirror optical floating zone furnace (Crystal Systems Co.). The phase purity of $EuTi_{1-x}Nb_xO_3$ ($x = 0.10$–0.20) was checked by powder x-ray diffraction (XRD) method using a high-resolution Rigaku TTRAX III diffractometer. The absence of any impurity peak in the XRD patterns of the powdered crystals, which are shown in Fig. 1, confirms the single-phase nature of the compounds. The structural analysis was done by the Rietveld refinement method using FULLPROF. The reflections in XRD patterns were indexed using the cubic $Pm\bar{3}m$ space group and the estimated lattice parameters are found to be comparable with that reported earlier [27]. Measurements of the temperature and field dependence of the dc magnetization were carried out in a superconducting quantum interference magnetometer (Quantum Design MPMS 3). The specific heat measurement was performed by the conventional relaxation technique in a physical property measurement system (Quantum Design). Resistivity was measured by a standard four-probe technique where the electrical contacts were made using highly conducting silver paint.

III. RESULTS AND DISCUSSIONS

Nb doping destabilizes the AFM ground state in $EuTiO_3$ and the system becomes FM above the doping level

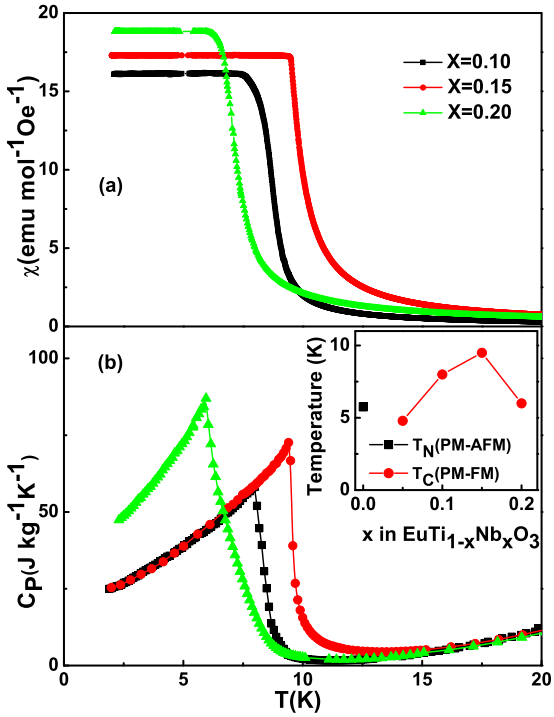

FIG. 2. (a) Thermal variation of zero-field-cooled susceptibility measured at 50 Oe and (b) heat capacity at low temperatures for $EuTi_{1-x}Nb_xO_3$ ($x = 0.10$–0.20) single crystals. Inset: Dependence of T_N and T_C on Nb doping concentration x in $EuTi_{1-x}Nb_xO_3$.

$x \sim 0.05$. Theoretical studies also reveal an intricate balance between nearest-neighbor AFM and next-nearest-neighbor FM interactions in $EuTiO_3$ [23]. The temperature dependence of dc magnetic susceptibility ($\chi = M/H$) and the specific heat for the studied ETNO ($x = 0.10$–0.20) single crystals are shown in Figs. 2(a) and 2(b), respectively. The T dependence of the zero-field-cooled magnetization and the λ-like heat capacity anomalies show that these samples undergo a continuous paramagnetic-to-ferromagnetic phase transition at Curie temperatures $T_C = 8$, 9.5, and 6 K for $x = 0.10$, 0.15, and 0.20, respectively. We have not observed any anomaly other than that at T_C either in magnetization or in heat capacity. This suggests that, unlike polycrystalline samples [27], the studied crystals are chemically homogeneous and AFM and FM phases do not coexist in the studied composition range.

T_C increases sharply with x, becomes a maximum around 0.15, and then decreases with further increase of x as shown in the inset of Fig. 2(b). This doping dependence of T_C is qualitatively similar to ELTO, though the maximum T_C is 1.5 K higher in ETNO [24]. The value of saturation magnetization at 2 K and 7 T is very close to the expected moment 7 μ_B/Eu. In the paramagnetic (PM) state, susceptibility obeys the Curie-Weiss (CW) law with effective moment, $P_{\text{eff}} = 7.9\,\mu_B$/Eu, and the CW temperature, $\theta_{\text{CW}} = 8$ K (for $x = 0.15$) [25]. To understand the correlation between transport and magnetism, the magnetic excitation spectrum has been investigated by estimating the spontaneous magnetization (M_S) using Arrott plots with field up to 7 T. Figure 3 shows the T dependence of M_S for the $x = 0.15$ sample as a representative. Well below the transition temperature, where the critical fluctuation is

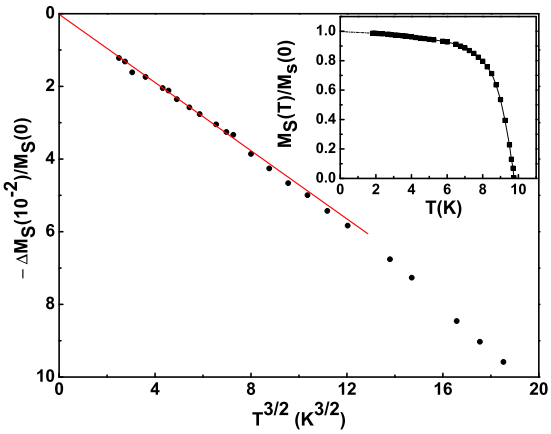

FIG. 3. $T^{3/2}$ dependence of ΔM_S for $x = 0.15$ crystal below T_C. Solid line is the fit to Bloch's law. Inset: Temperature dependence of M_S normalized at $T = 0$ K.

absent, the temperature variation of M_S can be explained by Bloch's $T^{3/2}$ law [29],

$$[M_S(0) - M_S(T)]/M_S(0) = \Delta M_S/M_S(0) = DT^{3/2}, \quad (1)$$

where D is the spin-wave parameter. For a simple cubic lattice, the coefficient D can be determined from the relation $D = (0.0587/S)(k_B/2JS)^{1.5}$, where J is the exchange coupling between two neighboring Eu^{2+} moments. Figure 3 shows that at low temperature ($T < 4$ K), $M_S(T)$ obeys Bloch's $T^{3/2}$ law. From the slope of the linear fit to the data, we obtain $D = 5 \times 10^{-3}$ $K^{-3/2}$ and the strength of the exchange interaction is estimated to be $0.3k_B$ K. This value of J is comparable to that predicted by molecular field theory [29], $J = 3k_BT_C/2ZS(S+1) = 0.15k_B$ K, where Z is the number of nearest-neighbor spins. For a simple cubic perovskite structure, $Z = 6$. Figure 4(a) depicts $\rho(T)$ curves for $EuTi_{1-x}Nb_xO_3$ single crystals. Over the entire temperature range, ρ exhibits metallic behavior ($d\rho/dT > 0$), except in a

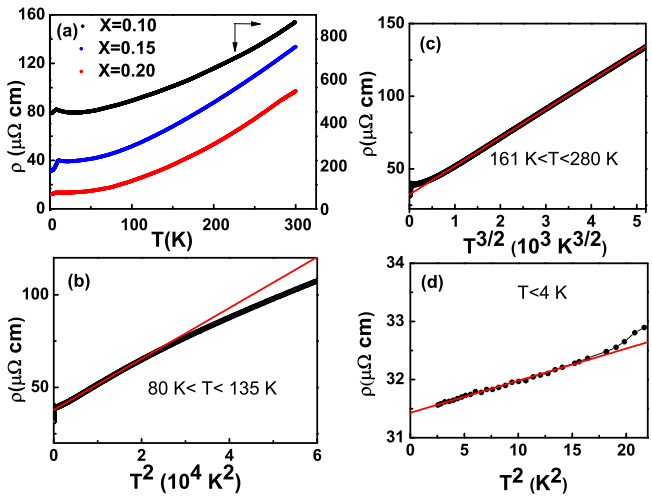

FIG. 4. (a) Temperature dependence of resistivity for all the three ETNO crystals. For $x = 0.15$ crystal, (b) T^2 dependence of ρ in the PM region, (c) $T^{3/2}$ variation of ρ in the PM region, and (d) T^2 fitting to ρ in the FM region.

narrow region just above T_C, where a weak increase in ρ has been observed with decreasing T for all the three samples. ρ drops sharply just below T_C due to the suppression of spin-disorder scattering. In the FM state, ρ decreases at a much faster rate with decreasing T as compared to that in the PM state. Though the qualitative nature of the $\rho(T)$ curve is similar to that in an earlier report on polycrystalline samples, for a given Nb content, the absolute value of ρ is smaller and the residual resistivity ratio $\rho(300\,\text{K})/\rho(2\,\text{K})$ is much larger in single crystals. For example, the values of $\rho(2\,\text{K})$ and $\rho(300\,\text{K})/\rho(2\,\text{K})$ are $150\,\mu\Omega$ cm and 1.5, respectively, for the polycrystalline sample [27] while the corresponding values are $12\,\mu\Omega$ cm and 8 for the single crystal, with $x = 0.20$. At low temperature, the large value of ρ in polycrystalline samples is due to the strong grain boundary scattering.

It is clear that the metallic behavior of $\rho(T)$ in the PM state cannot be fitted with a single power-law expression over the entire temperature range, because before ρ starts to increase a strong upward curvature develops at low temperature. To explain the intricate nature of the $\rho(T)$ curve, the role of different scattering mechanisms in charge conduction has been analyzed in detail. In the PM state, ρ exhibits a quadratic T dependence, $\rho = \rho_{a0} + aT^2$, in a narrow range above the minimum followed by a crossover to $\rho = \rho_{b0} + bT^{3/2}$ dependence over a wider range and up to temperatures as high as 280 K. The observed behavior of ρ is demonstrated in Figs. 4(b) and 4(c) for $x = 0.15$ as a representative. We have also analyzed the temperature dependence of ρ for $x = 0.10$ and 0.20 samples as shown in Figs. 8 and 9, respectively, in the Appendix. The deduced values of a and b in two different temperature ranges in the PM state are presented in Table I for all the three samples. The T^2 behavior of ρ is an indication of electronic correlation, consistent with the formation of a Fermi-liquid state. The coefficient a is a measure of the quasiparticle-quasiparticle scattering rate. As expected, a decreases rapidly with the increase in carrier doping. Often, metallic oxides are termed "bad metals" due to their strong electron-electron interaction. The deduced value of a for $x = 0.20$ is about an order of magnitude smaller than that for the well-known itinerant ferromagnet $SrRuO_3$ but two orders of magnitude larger than that for the elemental ferromagnets such as Fe, Co, and Ni [15].

ρ in several FM perovskites shows T^2 dependence. It is noteworthy that the T^2 dependence in these systems has been observed well below the T_C. ρ also exhibits T^2 dependence well below T_C for ETNO, as shown in Fig. 4(d) for $x = 0.15$. Contrary to the observed T^2 behavior of ρ in the PM state, T^2 behavior in the FM state results in unusually large value of the coefficient a, estimated to be more than one order of magnitude larger than that in the PM state. Such a huge difference in the values of a in PM and FM states indicates that the T^2 dependence of ρ in the FM state is due to the dominant magnetic scattering over the electron-electron scattering. In ferromagnets, ρ shows T^2 dependence due to the electron-magnon scattering. As both electron-electron and electron-magnon scattering occur at low temperature, it is very difficult to separate their relative contributions in resistivity for the FM materials with high Curie temperature. Even in elemental ferromagnets, where the electronic correlation is believed to be very weak, the origin of T^2 behavior of ρ

TABLE I. Estimated values of the resistivity coefficient a in units of $\mu\Omega\,\mathrm{cm/K^2}$ in the FM ($T < T_C$) and PM ($T > T_C$) states and the resistivity coefficient b in units of $\mu\Omega\,\mathrm{cm/K^{3/2}}$ in the PM state ($T > T_C$) for $EuTi_{1-x}Nb_xO_3$ single crystals with $x = 0.10$, 0.15, and 0.20. For $x = 0.20$, the accurate determination of the parameter a below T_C is not possible due to its low transition temperature.

x	a ($T < T_C$)	Range of T (K)	a ($T > T_C$)	Range of T (K)	b ($T > T_C$)	Range of T (K)
0.10	26.9×10^{-2}	$T < 2.9$	6.0×10^{-3}	$73 < T < 120$	8.4×10^{-2}	$175 < T < 260$
0.15	5.5×10^{-2}	$T < 4$	1.4×10^{-3}	$80 < T < 135$	2.0×10^{-2}	$161 < T < 280$
0.20			1.1×10^{-3}	$85 < T < 130$	1.7×10^{-2}	$150 < T < 233$

at low temperature is not yet settled [30]. Due to the much lower T_C of the studied system, we have been able to detect both scatterings, in two different temperature regions. Normally, in conventional metals, ρ shows linear T dependence at high temperatures due to the electron-phonon scattering. The observed crossover of the temperature dependence of the resistivity from T^2 to $T^{3/2}$ at high temperatures is quite unusual. To confirm that this $T^{3/2}$ dependence of ρ does not result due to a very sluggish crossover from T^2 to T dependence, a theoretical fit to the observed $\rho(T)$ can be done using the full Bloch-Grüneisen expression, which contains the electron-phonon resistivity contribution, $\rho_{e\text{-}ph}(T)$, and the residual resistivity, ρ_0, terms as follows:

$$\rho_{e\text{-}ph}(T) = \rho_0 + \rho'\left(\frac{T}{\theta_D}\right)^5 \int_0^{\frac{\theta_D}{T}} \frac{x^5 e^x}{(e^x - 1)^2} dx, \qquad (2)$$

where θ_D is the Debye temperature and ρ' is the coefficient for the T dependence of resistivity. We have tried to fit the resistivity above the minima and observed that neither the full Bloch-Grüneisen expression nor the addition of an extra term aT^n to Eq. (2) reproduces the experimental data. However, the $\rho(T)$ curve fits well at high temperatures for $n = 3/2$ as shown in Fig. 5 for $x = 0.20$. Figure 5 also shows that the contribution of $T^{3/2}$ is significantly larger than the Bloch-Grüneisen expression for electron-phonon scattering, which implies that $T^{3/2}$ dependence dominates the charge conduction mechanism in the present system. This is also clear from Figs. 8(c) and 9(c) in the Appendix. ρ shows a weak upward deviation from $T^{3/2}$ dependence at high temperatures. Generally, the deviation from T^2 dependence of the resistivity

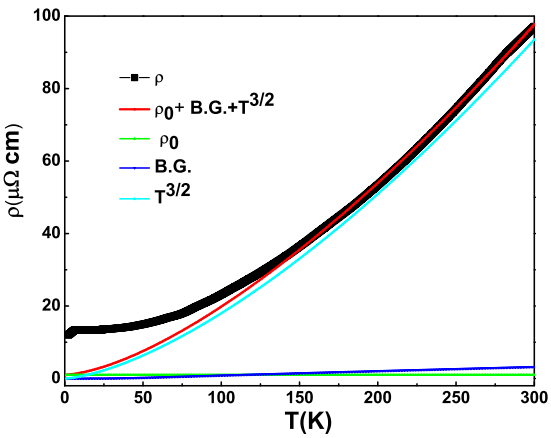

FIG. 5. For an $x = 0.20$ crystal, a theoretical fit to the observed $\rho(T)$ using the full Bloch-Grüneisen expression [Eq. (2)] with $bT^{3/2}$ in the PM region (red line).

at low temperature is one of the hallmarks of non-Fermi-liquid (NFL) behavior in itinerant systems as ample experimental evidences have been presented in heavy-fermion systems. An obvious origin of this is the vicinity of the quantum critical point where the quantum critical dynamics results in an unusual temperature dependence of the resistivity, heat capacity, magnetic susceptibility, etc. [31]. However, generic NFL behavior of the resistivity has been found in some itinerant magnets with ferromagnetic, helical, or skyrmionic order both near and away from the magnetic transition and very recently its origin has been investigated theoretically, which rules out the possible influence of quantum critical behavior [32]. Therefore, unlike the heavy-fermion systems, in many oxides [15,33,34] like $SrRuO_3$ and the present system, no such hallmarks of the NFL behavior have been observed in the specific heat and magnetic susceptibility. This generic NFL behavior is still far from understood and very challenging to explain. In this context, below we compare and contrast our results with the $T^{3/2}$ or $T^{5/3}$ dependence of the resistivity, observed away from the magnetic transitions, reported in some oxide and intermetallic itinerant systems.

ρ for a weakly and nearly FM metal has been predicted to show T^2 dependence at $T \ll T_C$ and $T^{5/3}$ dependence in the vicinity of T_C [35,36]. This behavior has been observed in weak itinerant ferromagnets $Ni_{75\pm x}Al_{25\pm x}$ [37]. For a three-dimensional AFM system, $T^{3/2}$ dependence of ρ is expected to occur in the vicinity of the AFM transition due to the spin fluctuations. In systems like Pd-based dilute alloys such as PdFe and PdMn (with a few percent of Fe or Mn), the observed $T^{3/2}$ dependence of ρ well below the transition temperature is attributed to the incoherent part of the electron-magnon scattering [38]. Thus, $T^{3/2}$ behavior of ρ well above the FM transition for the present ETNO system cannot be interpreted in terms of incoherent electron-magnon scattering.

The transport properties of $RNiO_3$, another strongly correlated system with single valance Ni^{3+}, have become of great interest recently [9,10,39]. ρ follows T^n ($n = 1.33$ and 1.6) behavior in single crystals of $PrNiO_3$ under high pressure, whereas in ultrathin epitaxial films of $NdNiO_3$, ρ is extremely sensitive to lattice strain and for highly compressive strained films, ρ shows $T^{5/3}$ dependence at high temperatures [9,10]. In itinerant ferromagnets Ni_xPd_{1-x}, $\rho(T)$ shows $T^{5/3}$ dependence up to as high as 150 K [31]. However, in Nd-doped $LaNiO_3$, ρ shows $T^{3/2}$ behavior [39]. The $T^{3/2}$ dependence of ρ has also been observed in the well-known skyrmion lattice system MnSi under high pressure [12,13]. The deviation from T^2 dependence of ρ in these systems has been attributed to the non-Fermi-liquid state. The $T^{3/2}$ behavior of ρ has also been reported in single crystals and thin films of the itinerant ferromagnet $SrRuO_3$ [15,34]. In $SrRuO_3$, ρ exhibits T^2

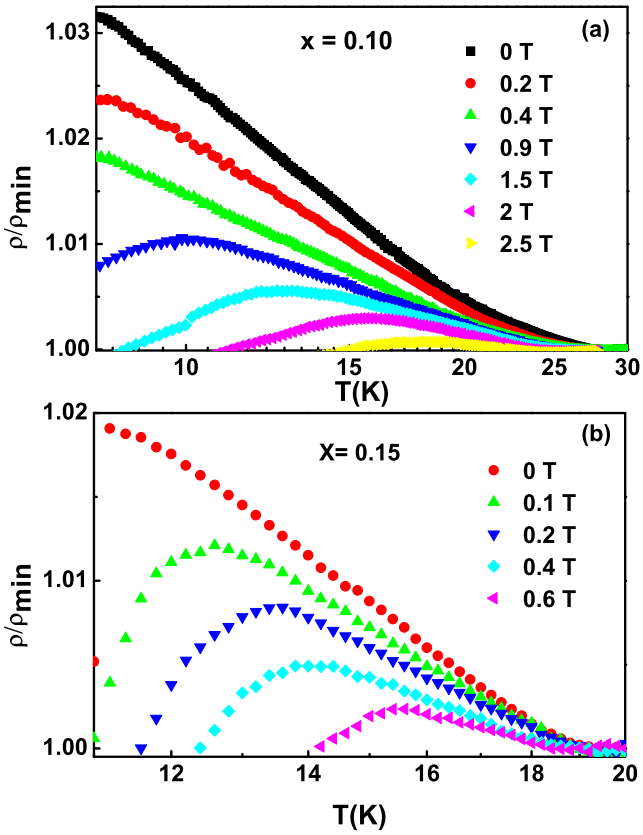

FIG. 6. The $\log(T)$ dependence of ρ in the temperature window $T_C < T < T_{min}$ at different magnetic fields for the (a) $x = 0.10$ and (b) $x = 0.15$ crystals.

dependence well below T_C (∼160 K) and a crossover to $T^{3/2}$ dependence occurs with increasing T. Similar to ETNO, $T^{3/2}$ behavior is observed at high temperature over a wide range. This crossover from T^2 to $T^{3/2}$ dependence of ρ in $SrRuO_3$ has been attributed to the non-Fermi-liquid transition [34]. The values of the coefficient b deduced from the ρ-vs-$T^{3/2}$ plot are comparable to that reported for $SrRuO_3$ [34]. The exponent n is found to be sensitive to the underlying phenomena giving rise to the critical fluctuations associated with non-Fermi-liquid behavior. The widely observed critical exponent 3/2 indicates finite wave-vector fluctuations [9].

We have already mentioned that the $\rho(T)$ curve for all the three compositions displays a broad minimum at T_{min} in the PM state [Fig. 4(a)]. In the temperature window $T_C < T < T_{min}$, $\rho(T)$ is observed to follow $\log(T)$ dependence as shown in Figs. 6(a) and 6(b). The effect of magnetic field on the $\log(T)$ dependence of ρ has also been studied and is shown in Figs. 6(a) and 6(b) for $x = 0.10$ and 0.15, respectively. For $x = 0.20$, the increase of ρ below T_{min} is very small and, as a result, the fit is insensitive. Figures 6(a) and 6(b) show that with the increase in H, ρ decreases rapidly, the minimum shifts toward lower temperature, and the range of $\log(T)$ behavior shrinks progressively. This clearly indicates that the upturn in ρ below T_{min} is due to the Kondo scattering of the itinerant electrons by the localized $4f$ spins of the Eu^{2+}.

It has been suggested that the ferromagnetism in ELTO and ETNO is mediated by the Ruderman-Kittle-Kasuya-Yosida (RKKY) exchange interaction between the itinerant d electrons of Ti or Nb and the localized $4f$ moments of Eu^{2+}[22,24,27]. Thus, the competition of the intersite RKKY exchange interaction, $E_{RKKY} = J^2\eta$, where η is the density of states of the conduction sea, and the Kondo temperature, $T_K \sim D_W e^{-1/(2J\eta)}$, where D_W is the bandwidth, results in the formation of either the usual magnetic ordering with large moments, viz., in rare-earth elements or the nonmagnetic Kondo state with suppressed moments [40,41]. For small $J\eta$, $E_{RKKY} \gg T_K$, the dominant RKKY-type FM exchange below T_C stabilizes the usual magnetic ordering with the full moment of Eu^{2+} in ETNO and ELTO. The sign and strength of the RKKY exchange interaction ($J_{RKKY} \sim \cos(2k_F r)/r^3$) depend on the spatial separation (r) of the localized moments (Eu^{2+}) and the Fermi wave vector k_F. As k_F and r are functions of Nb doping, the two energy scales are changing with increasing x. The estimated lattice parameter a for different doping level x shows that the spatial separation between the Eu^{2+} moments increases almost linearly with increasing x (Fig. 1). The variation of the transition temperatures (T_N or T_C) with the doping concentration x shows an oscillatory behavior; i.e., the exchange interaction changes sign with increasing doping [inset of Fig. 2(b)] and is thereby consistent with the RKKY picture. At around $x = 0.15$, the suppression of Kondo scattering by FM RKKY exchange is largest and that is why T_C peaks around $x = 0.15$. Similar behavior has also been observed in La- and Gd-doped $EuTiO_3$ crystals, which has been ascribed to RKKY oscillation [22]. The low temperature and high field favor the FM phase and prevent the formation of Kondo singlets; thereby the range of $\log(T)$ fit shrinks as the FM phase intrudes into the high-T phase with applied field. Therefore, $\rho(T)$ of the present ETNO system mimics the behavior of a FM Kondo lattice, which is relatively less numerous and exhibits rather complicated physical pictures [40–42]. In general, the Kondo effect is strongly suppressed in systems with large local moments. Several rare-earth-based AFM systems with RKKY interaction exhibit a minimum in $\rho(T)$ which cannot be explained by the Kondo scattering but is ascribed to the formation of a liquidlike spin state [43–46]. We would like to mention that few Eu- and Sm-based compounds also show the Kondo effect but they order antiferromagnetically [47–49].

The sharp anomaly at T_C in the $\rho(T)$ curve weakens with increase in H and disappears above a critical field and ρ shows metallic behavior over the entire range of T, as shown in Fig. 7(a) for the $x = 0.15$ sample. This suggests that the conduction electron is strongly coupled with localized Eu^{2+} spin. MR defined as $\Delta\rho/\rho = [(\rho(H) - \rho(0))/\rho(0)]$, is small and negative, except in the vicinity of T_C. The T and H dependence of MR of ETNO and its value are similar to that reported for ELTO [22]. We have also measured $\Delta\rho/\rho$ in both electron-magnon and electron-electron scattering dominated regions. Well below T_C, where electron-magnon scattering dominates ρ, $\Delta\rho(H)/\rho$ increases rapidly with field and then starts to saturate at high field as shown in Fig. 7(b) for some representative temperatures. The qualitative nature of $\Delta\rho(H)/\rho$ is similar to the $M(H)$ curve and to that calculated theoretically for spin-wave scattering [36]. Also, $\Delta\rho/\rho$ approximately scales with the magnetization offset $\Delta M_S/M_S(0)$ at low temperature where ρ tends to saturate with field. These

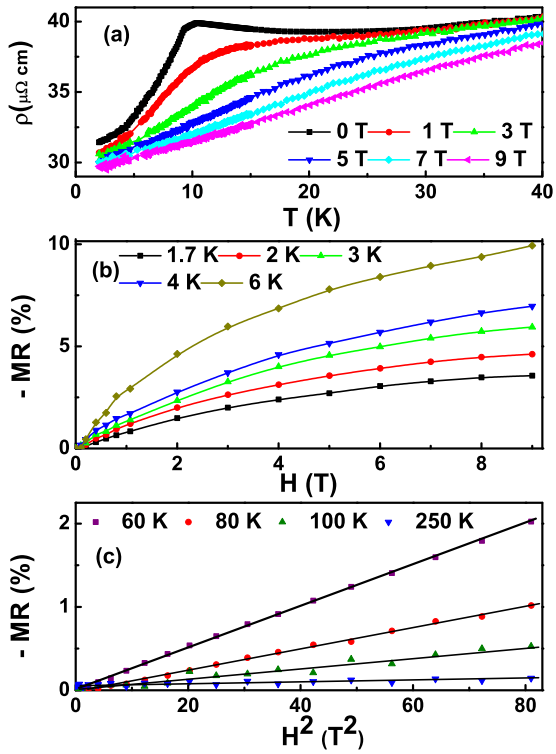

FIG. 7. (a) Temperature dependence of the resistivity for different magnetic fields. (b) MR versus H below T_C and (c) H^2 dependence of the MR well above T_C for the $x = 0.15$ crystal. Solid black lines correspond to a linear fit.

observations support spin-wave scattering. Contrary to this, the nature of $\Delta\rho(H)/\rho$ curves well above T_C in Fig. 7(c) is very different. $\Delta\rho/\rho$ is very small and shows H^2 dependence. This relation comes into play as the carriers get scattered by the thermally fluctuating spins. As M increases with H, the fluctuation of spins decreases, leading to a negative MR.

When Eu^{2+} is replaced by La^{3+} or Gd^{3+}, electrons are introduced in $3d$ t_{2g} orbitals of Ti, which leads to mixed valence Ti^{3+} and Ti^{4+} and the metallic conductivity arises due to the hopping of electrons from $3d^1$ to $3d^0$. In ABO_3 perovskites, substitution at site A by some heterovalent element transfers either a hole or an electron from A to transition metal B and the system becomes metallic above a critical doping. On the other hand, insulator-to-metal transition through B-site substitution is rare because substitution at this site creates disordering, which favors the localization effect. Thus, the insulator-to-metal transition with substitution of a small amount of Nb (∼5%) at the Ti site suggests that charge conduction is not due to the percolation through Nb ions. The unpaired $4d^1$ electron of Nb hops to the empty $3d^0$ orbital of Ti and, as a result, the $4d$ state of Nb^{4+} strongly hybridizes with $3d$ of Ti^{4+}. At higher doping level x close to 1, Nb is surrounded by other Nb ions, and in such a case conductivity is dominated by the hopping of electrons between isovalent Nb ions and makes $EuNbO_3$ metallic. Unlike $EuNbO_3$, the end members of $EuTiO_3$ are Mott insulators when substitution is done at the Eu site with other rare-earth ions.

The charge conduction mechanism in strongly correlated transition-metal oxides is very different from that of good elemental metals, and heavy fermions. Several nonmagnetic metallic oxides such as $La_{1-x}Sr_xTiO_3$ (LSTO), $LaNiO_3$ (LNO), $SrVO_3$ (SVO), $CaVO_3$ (CVO), and $SrTi_{1-x}Nb_xO_3$ (STNO), with perovskite structure similar to ETNO, exhibit T^2 dependence of ρ due to electron-electron scattering [1,10,50]. The T^2 dependence of ρ in these systems is strong and extends over a wide range. For example, ρ shows T^2 dependence up to as high as 300 K for LSTO, CVO, and SVO [1]. In $Nd_{2-x}Ce_xCuO_4$, ρ shows T^2 behavior up to about 700 K and then crosses over to T dependence [51]. This suggests that electron-phonon scattering in these systems is very weak as compared to electron-electron scattering. In ETNO also, the electron-phonon scattering is very weak and appears at high temperatures. Furthermore, the value of the coefficient a for the above-mentioned compounds is found to be very close to that for ETNO ($\sim 10^{-3}$ $\mu\Omega$ cm K^{-2}) in the PM state at their equivalent carrier density ($\sim 2 \times 10^{21}$ cm^{-3}) [1,52]. It is worth comparing the behavior of the T dependence of ρ of ETNO with STNO because in both the cases the charge carrier is doped by substituting Nb at Ti sites. a is observed to scale with carrier density over a wide range for doped $SrTiO_3$ and its value is about 10^{-3} $\mu\Omega$ cm K^{-2} at the corresponding carrier density of ETNO [1,50]. On the other hand, the observed values of a for ETNO below 4 K do not fall on the scaling plot. This allows us to conclude that the value of the coefficient a below 4 K is too large to be electron-electron scattering for such a high carrier density. However, in these nonmagnetic transition-metal oxides, ρ does not show any crossover from T^2 to $T^{3/2}$ dependence with increasing temperature. Thus, we can say that the non-Fermi-liquid behavior in ETNO is of magnetic origin as in the case of $SrRuO_3$.

IV. CONCLUSIONS

In summary, we report a comprehensive study of the transport properties in single-crystalline $EuTi_{1-x}Nb_xO_3$ itinerant ferromagnets. The observed T^2 dependence of the resistivity in the FM state is due to the dominant electron-magnon scattering, unlike that observed in the PM state, which is due to the electron-electron scattering. Also, a crossover from a T^2 to $T^{3/2}$ temperature dependence of the resistivity has been observed in the PM state, suggesting a non-Fermi-liquid behavior. Furthermore, the scattering of the itinerant electrons by the large localized moments of the Eu^{2+} ions results in a Kondo-like upturn in the resistivity above T_C. The presence of several scattering mechanisms and the non-Fermi-liquid behavior make ETNO a unique ferromagnetic metallic system.

ACKNOWLEDGMENTS

We thank R. Singha, S. Roy, M. Das, A. Pariari, and A. Paul for their help during experimental measurements. Also, we would like to thank B. Banerjee for his help in theoretical fitting.

APPENDIX

The thermal variation of resistivity of the ETNO compounds with $x = 0.10$ and $x = 0.20$ is shown in Figs. 8 and 9, respectively. Similar to $EuTi_{0.85}Nb_{0.15}O_3$, the resistivity for

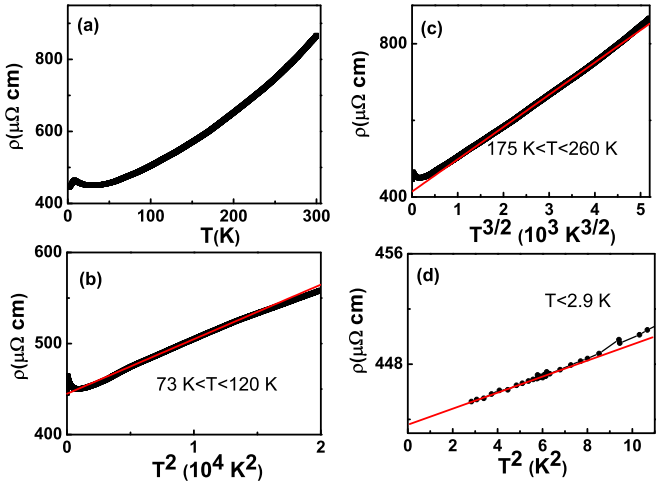

FIG. 8. (a) Temperature dependence of the resistivity of the $EuTi_{1-x}Nb_xO_3$ ($x = 0.10$) compound over the whole temperature range. (b) T^2 dependence of resistivity in the paramagnetic region in the temperature range from 73 to 120 K. (c) $T^{3/2}$ variation of resistivity in the temperature range $175 < T < 260$ K above T_C and (d) T^2 fitting into the resistivity at very low temperature in the ferromagnetic region below 2.9 K.

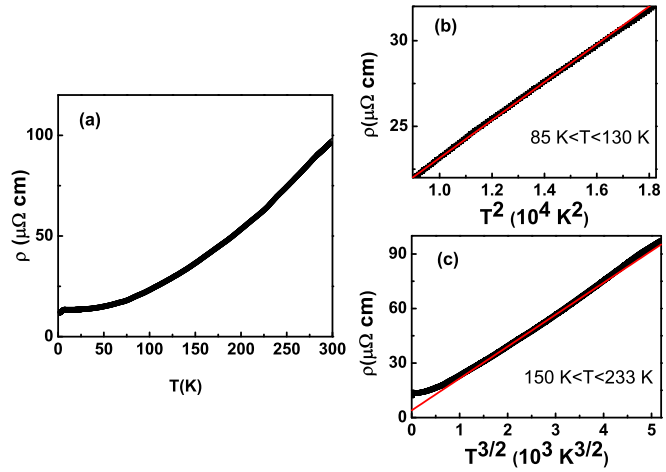

FIG. 9. (a) Temperature dependence of the resistivity of the $EuTi_{1-x}Nb_xO_3$ ($x = 0.20$) compound over the whole temperature range. (b) T^2 dependence of resistivity in the temperature range $85 < T < 130$ K above T_C. (c) $T^{3/2}$ variation of resistivity in the temperature range $150 < T < 233$ K above T_C.

both of the compounds obeys different power laws of temperature for different temperature regimes. They also exhibit T^2 and $T^{3/2}$ behavior in the paramagnetic region above T_C.

But due to having lower magnetic transition temperature we are unable to fit the resistivity of the $x = 0.20$ compound with T^2 over a reasonable interval of T below T_C for the accurate determination of the parameter a.

[1] M. Imada, A. Fujimori, and Y. Tokura, Rev. Mod. Phys. **70**, 1039 (1998).
[2] L. Klein, J. S. Dodge, C. H. Ahn, J. W. Reiner, L. Mieville, T. H. Geballe, M. R. Beasley, and A. Kapitulnik, J. Phys.: Condens. Matter. **8**, 10111 (1996).
[3] M. Vojta, Rep. Prog. Phys. **66**, 2069 (2003).
[4] M. Brando, D. Belitz, F. M. Grosche, and T. R. Kirkpatrick, Rev. Mod. Phys. **88**, 025006 (2016).
[5] S. A. Grigera, R. S. Perry, A. J. Schofield, M. Chiao, S. R. Julian, G. G. Lonzarich, S. I. Ikeda, Y. Maeno, A. J. Millis, and A. P. Mackenzie, Science **294**, 329 (2001).
[6] J. Kondo, Prog. Theor. Phys. **27**, 772 (1962).
[7] P. Nozieres, *Theory of Interacting Fermi Systems* (Benjamin, New York, 1964).
[8] R. P. Smith, M. Sutherland, G. G. Lonzarich, S. S. Saxena, N. Kimura, S. Takashima, M. Nohara, and H. Takagi, Nature (London) **455**, 1220 (2008).
[9] J. Liu, M. Kargarian, M. Kareev, B. Gray, P. J. Ryan, A. Cruz, N. Tahir, Y.-D. Chuang, J. Guo, J. M. Rondinelli, J. W. Freeland, G. A. Fiete, and J. Chakhalian, Nat. Commun. **4**, 2714 (2013).
[10] J.-S. Zhou, J. B. Goodenough, and B. Dabrowski, Phys. Rev. Lett. **94**, 226602 (2005).
[11] Q. Si and F. Steglich, Science **329**, 1161 (2010).
[12] C. Pfleiderer, S. R. Julian, and G. G. Lonzarich, Nature (London) **414**, 427 (2001).
[13] C. Pfleiderer, D. Reznik, L. Pintschovius, H.v. Löhneysen, M. Garst, and A. Rosch, Nature (London) **427**, 227 (2004).
[14] J. Custers, P. Gegenwart, H. Wilhelm, K. Neumaier, Y. Tokiwa, O. Trovarelli, C. Geibel, F. Steglich, C. Pépin, and P. Coleman, Nature (London) **424**, 524 (2003).
[15] L. Klein, J. S. Dodge, C. H. Ahn, G. J. Snyder, T. H. Geballe, M. R. Beasley, and A. Kapitulnik, Phys. Rev. Lett. **77**, 2774 (1996).
[16] G. Koster, L. Klein, W. Siemons, G. Rijnders, J. S. Dodge, C.-B. Eom, D. H. A. Blank, and M. R. Beasley, Rev. Mod. Phys. **84**, 253 (2012).
[17] E. A. Yelland, S. J. C. Yates, O. Taylor, A. Griffiths, S. M. Hayden, and A. Carrington, Phys. Rev. B **72**, 184436 (2005).
[18] Z. Y. Zhao, O. Khosravani, M. Lee, L. Balicas, X. F. Sun, J. G. Cheng, J. Brooks, H. D. Zhou, and E. S. Choi, Phys. Rev. B **91**, 161106(R) (2015).
[19] G. Khaliullin and S. Okamoto, Phys. Rev. Lett. **89**, 167201 (2002).
[20] J. Hemberger, H.-A. Krug von Nidda, V. Fritsch, J. Deisenhofer, S. Lobina, T. Rudolf, P. Lunkenheimer, F. Lichtenberg, A. Loidl, D. Bruns, and B. Büchner, Phys. Rev. Lett. **91**, 066403 (2003).
[21] C. Ulrich, A. Gössling, M. Grüninger, M. Guennou, H. Roth, M. Cwik, T. Lorenz, G. Khaliullin, and B. Keimer, Phys. Rev. Lett. **97**, 157401 (2006).
[22] T. Katsufuji and Y. Tokura, Phys. Rev. B **60**, R15021 (1999).
[23] T. Katsufuji and H. Takagi, Phys. Rev. B **64**, 054415 (2001).
[24] K. S. Takahashi, M. Onoda, M. Kawasaki, N. Nagaosa, and Y. Tokura, Phys. Rev. Lett. **103**, 057204 (2009).
[25] S. Roy, N. Khan, and P. Mandal, APL Mater. **4**, 026102 (2016).

[26] L. Li, J. R. Morris, M. R. Koehler, Z. Dun, H. Zhou, J. Yan, D. Mandrus, and V. Keppens, Phys. Rev. B **92**, 024109 (2015).
[27] L. Li, H. Zhou, J. Yan, D. Mandrus, and V. Keppens, APL Mater. **2**, 110701 (2014).
[28] V. G. Zubkov, A. P. Tyutyunnik, V. A. Pereliaev, G. P. Shveikin, J. Kohler, R. K. Kremer, A. Simon, and G. Svensson, J. Alloys Compd. **226**, 24 (1995).
[29] C. Kittel, *Introduction to Solid State Physics* (Wiley, New York, 2005).
[30] P. V. Prakash Madduri and S. N. Kaul, Phys. Rev. B **95**, 184402 (2017).
[31] M. Nicklas, M. Brando, G. Knebel, F. Mayr, W. Trinkl, and A. Loidl, Phys. Rev. Lett. **82**, 4268 (1999).
[32] T. R. Kirkpatrick and D. Belitz, Phys. Rev. B **97**, 064411 (2018).
[33] F. Rivadulla, J.-S. Zhou, and J. B. Goodenough, Phys. Rev. B **67**, 165110 (2003).
[34] L. M. Wang, H. E. Horng, and H. C. Yang, Phys. Rev. B **70**, 014433 (2004).
[35] K. Ueda and T. Moriya, J. Phys. Soc. Jpn. **39**, 605 (1975).
[36] S. N. Kaul, J. Phys.: Condens. Matter **17**, 5595 (2005).
[37] A. C. Abhyankar and S. N. Kaul, J. Phys.: Condens. Matter **20**, 445227 (2008).
[38] D. L. Mills, A. Fert, and I. A. Campbell, Phys. Rev. B **4**, 196 (1971).
[39] J. Blasco and J. A. Garcia, J. Phys.: Condens. Matter. **6**, 10759 (1994).
[40] C. Krellner, N. S. Kini, E. M. Brüning, K. Koch, H. Rosner, M. Nicklas, M. Baenitz, and C. Geibel, Phys. Rev. B **76**, 104418 (2007).
[41] V. N. Nikiforov, M. Baran, A. Jedrzejczak, and V. Y. Irkhin, Eur. Phys. J. B. **86**, 238 (2013).
[42] N. Takeda and M. Ishikawa, J. Phys.: Condens. Matter **15**, L229 (2003).
[43] Z. Wang, K. Barros, G. W. Chern, D. L. Maslov, and C. D. Batista, Phys. Rev. Lett. **117**, 206601 (2016).
[44] V. Fritsch, J. D. Thompson, and J. L. Sarrao, Phys. Rev. B **71**, 132401 (2005).
[45] E. V. Sampathkumaran, K. Sengupta, S. Rayaprol, K. K. Iyer, Th. Doert, and J. P. F. Jemetio, Phys. Rev. Lett. **91**, 036603 (2003).
[46] R. Mallik, E. V. Sampathkumaran, M. Strecker, and G. Wortmann, Europhys. Lett. **41**, 315 (1998).
[47] Y. Hiranaka, A. Nakamura, M. Hedo, T. Takeuchi, A. Mori, Y. Hirose, K. Mitamura, K. Sugiyama, M. Hagiwara, T. Nakama, and Y. Ōnuki, J. Phys. Soc. Jpn. **82**, 083708 (2013).
[48] A. Nakamura, T. Okazaki, M. Nakashima, Y. Amako, K. Matsubayashi, Y. Uwatoko, S. Kayama, T. Kagayama, K. Shimizu, T. Uejo, H. Akamine, M. Hedo, T. Nakama, Y. Ōnuki, and H. Shiba, J. Phys. Soc. Jpn. **84**, 053701 (2015).
[49] M. B. Maple, L. E. DeLong, and B. C. Sales, in *Handbook on the Physics and Chemistry of Rare Earths*, edited by K. A. Gschneidner and L. Eyring (North-Holland, Amsterdam, 1978), p. 797.
[50] X. Lin, B. Fauqué, and K. Behnia, Science **349**, 945 (2015).
[51] T. Sarkar, R. L. Greene, and S. Das Sarma, arXiv:1805.08360.
[52] Y. Kususe, H. Murakami, K. Fujita, I. Kakeya, M. Suzuki, S. Murai, and K. Tanaka, Jpn. J. Appl. Phys. **53**, 05FJ07 (2014).